Electronic Supplementary Information

Insights into dynamic structural evolution and its sodium storage mechanisms of P2/P3 composite cathode materials for sodium-ion batteries

Yi-Feng Liu,‡[a] Hai-Yan Hu,‡[b, c] Yan-Fang Zhu,*[b, c] Dan-Ni Peng,[a] Jia-Yang Li,[c] Yan-Jiang Li,[c] Yu Su,[c] Rui-Ren Tang,*[a] Shu-Lei Chou*[b,c] and Yao Xiao*[b, c]

[a] College of Chemistry and Chemical Engineering, Central South University, Changsha, Hunan 410083, China. Email: trr@csu.edu.cn

[b] College of Chemistry and Materials Engineering, Wenzhou University, Wenzhou, 325035, P.R. China

Email: yanfangzhu@wzu.edu.cn; chou@wzu.edu.cn; xiaoyao@wzu.edu.cn.

[c] Wenzhou Key Laboratory of Sodium-Ion Batteries, Wenzhou University Technology Innovation Institute for Carbon Neutralization, Wenzhou, 325035, P.R. China.

‡ These authors contributed equally to this work.

Experimental section

Material synthesis. The cathode materials $Na_{0.44}Mn_{0.7}Co_{0.3}O_2$ (referred to as NaMC-0.3) and $Na_{0.44}Mn_{0.5}Co_{0.5}O_2$ (NaMC-0.5) were synthesized via a method combining thermal polymerization with solid-state high-temperature steering. Initially, sodium acetate (CH_3COONa, Sigma-Aldrich, 99.00%), cobalt acetate $(CoCH_3COO)_2 \cdot 4H_2O$, Sigma-Aldrich, 99.90%), and manganese acetate $(Mn(CH_3COO)_2 \cdot 4H_2O$, Sigma-Aldrich, purity 99.99%) were dissolved in deionized water to create 0.4 M solution precursors. Stoichiometric amounts of acrylic acid (AA) and a specific quantity of nitric acid (HNO_3) were added to the mixture, resulting in AA-H_2O solutions with a 1:2 volume ratio. The solutions were heated at 180°C for 10 hours to promote the polymerization reaction, resulting in the formation of fluffy xerogels. The xerogels were ground for 10 minutes and then calcined at 550°C for 6 hours to remove organic components. Finally, the samples were sintered at 900°C for 12 hours to produce the final powder products.

Material Characterizations. X-ray diffraction (XRD) patterns were obtained using a D8 Advance Diffractometer (Bruker, Germany) equipped with a Cu Kα radiation source ($\lambda 1$ = 1.54056 Å, $\lambda 2$ = 1.54439 Å) over a 2θ range of 10°–70°. *In situ* XRD analysis was conducted using a specialized Swagelok cell with an aluminum foil window for X-rays. Morphological and structural characteristics were examined using field-emission scanning electron microscopy (SEM, SU-8020, Hitachi Limited, Japan).

Electrochemical tests. During half-cell assembly, the working electrode consisted of a homogeneous mixture comprising 70% active substance by weight, 20% Super P carbon, and 10% polyvinylidene difluoride (PVDF) binder, all mixed in N-methyl-2-pyrrolidone (NMP). The mixture was subsequently coated onto clean aluminium foil and dried under vacuum at 80°C overnight.

CR2032 coin cells were constructed within an argon-filled glove box, utilizing sodium foil and a porous glass fiber as the counter electrode and the separator, respectively. The selected electrolyte was a 1 M $NaClO_4$ solution in propylene carbonate (PC), supplemented with a 5% volume concentration of fluoroethylene carbonate (FEC) as an additive. Electrochemical assessments were performed using a Neware battery test system (CT-4008, Shenzhen, China) for battery analysis (1C = 120 mA g^{-1} in 2.0-4.0 V and 1C = 200 mA g^{-1} in 1.5-4.3 V). CV measurements were conducted using a Princeton instrument testing system. In the full-cell system, an anodic material was prepared from a blend of hard carbon, Super P carbon, and PVDF in a weight ratio of 8:1:1, and pre-sodiated via electrochemical methods (1C = 300 mA g^{-1}). The balancing of the mass between the anode and cathode was adjusted based on their respective reversible capacities. Current density was calculated based on the cathode mass (1C = 120 mA g^{-1}), with testing performed in the voltage range of 1.9–3.9 V at room temperature.

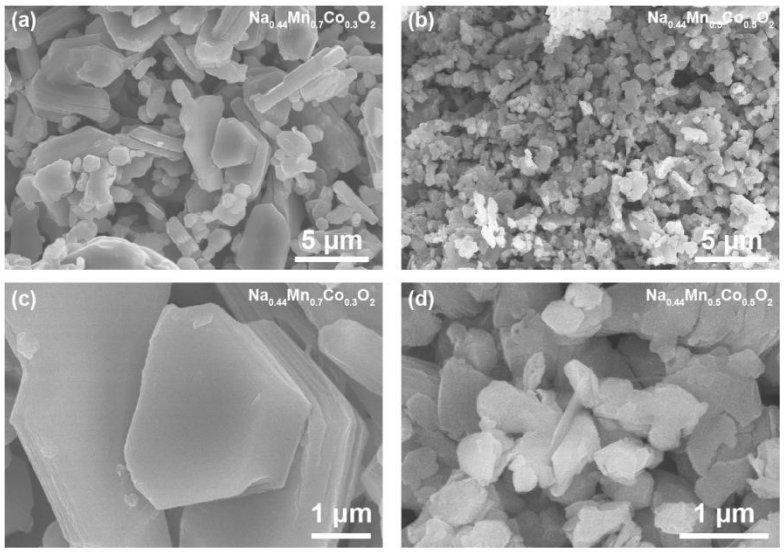

Figure S1. SEM images of (a, c) NaMC-0.3 and (b, d) NaMC-0.5 cathode materials at various magnifications.

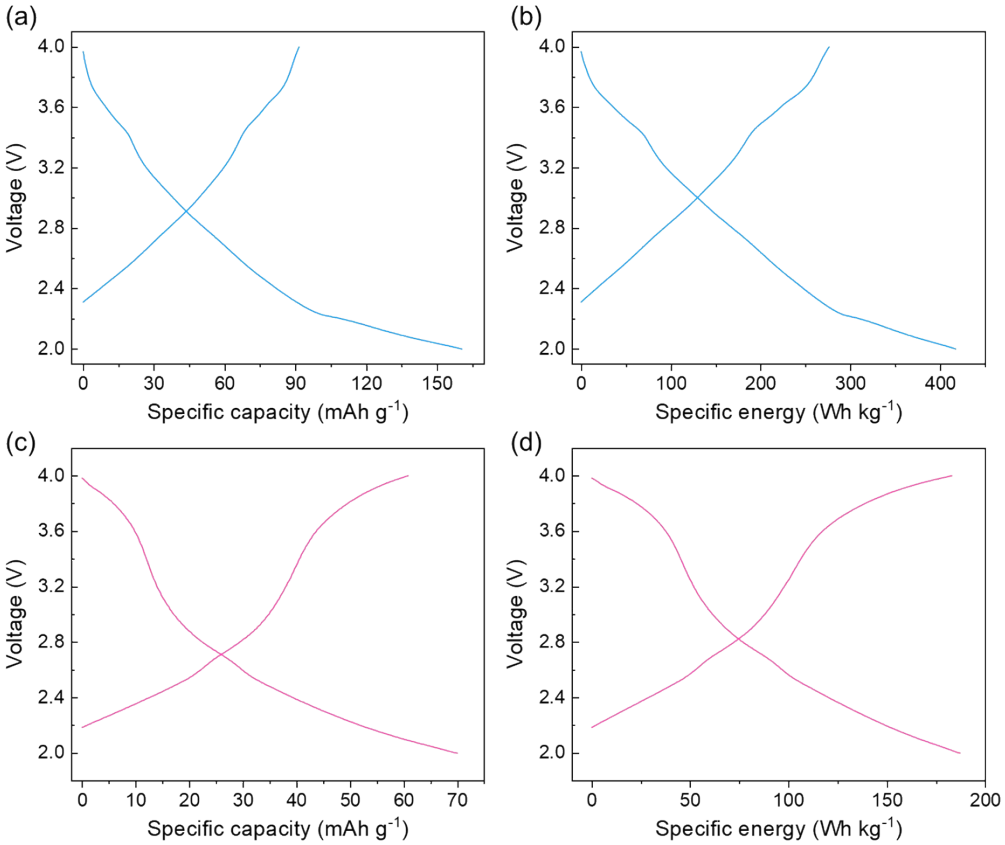

Figure S2. Initial galvanostatic charge/discharge curves for (a, b) NaMC-0.3 and (c, d) NaMC-0.5 electrodes in the voltage range of 2.0–4.0 V.

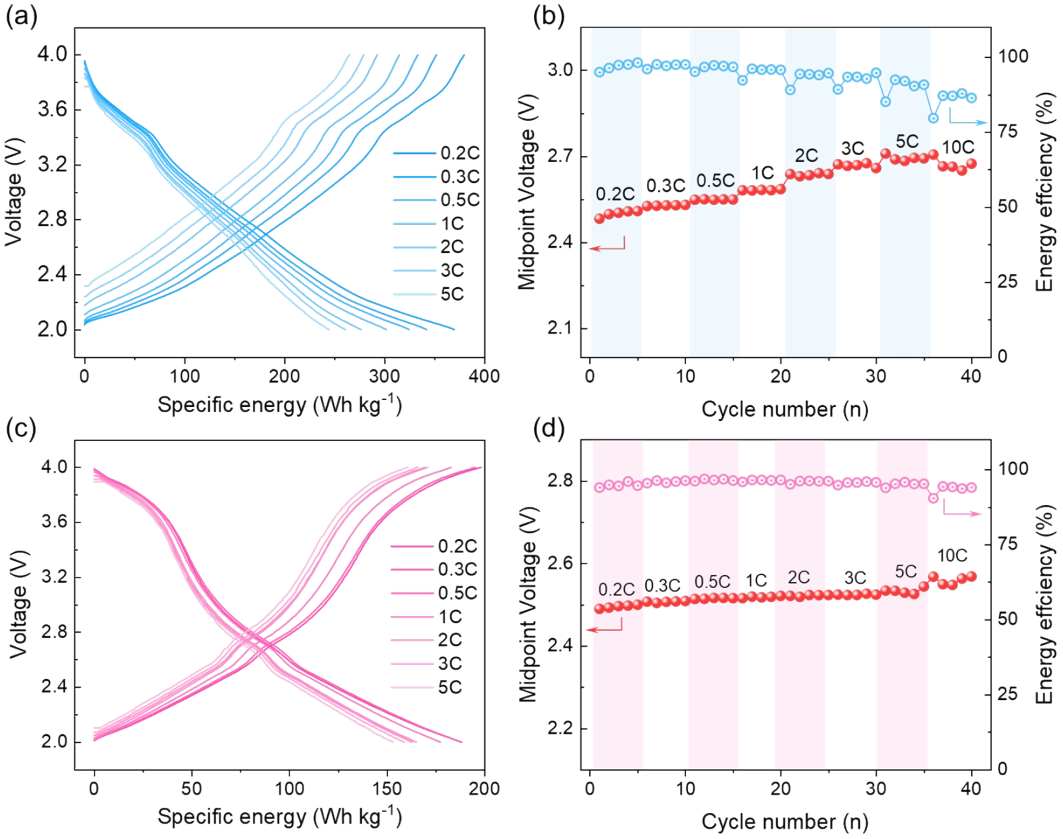

Figure S3. Rate performance for half-cell system: (a, c) Galvanostatic charge/discharge curves of NaMC-0.3 and NaMC-0.5 electrodes versus specific energy at various rates in the voltage range of 2.0–4.0 V, respectively. (b, d) Corresponding Midpoint voltage as well as energy efficiency of NaMC-0.3 and NaMC-0.5 electrodes, respectively.

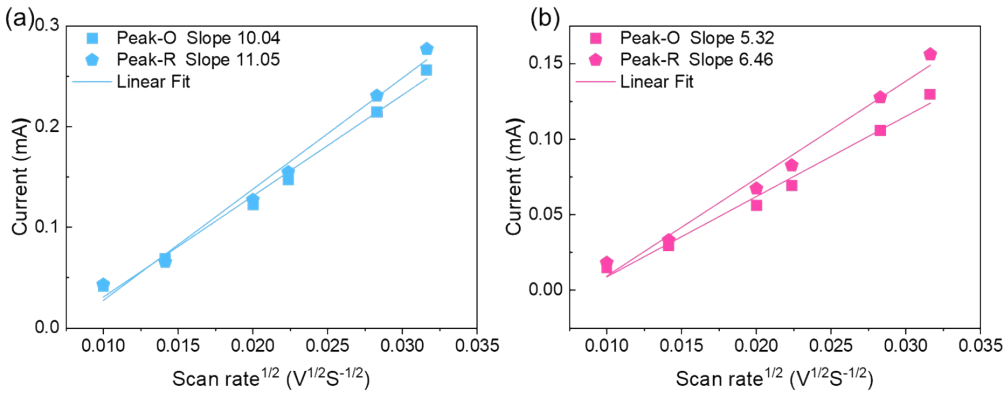

Figure S4. (a, b) Linear fitting of peak current versus square root of the scan rate of NaMC-0.3 and NaMC-0.5 electrodes, respectively.

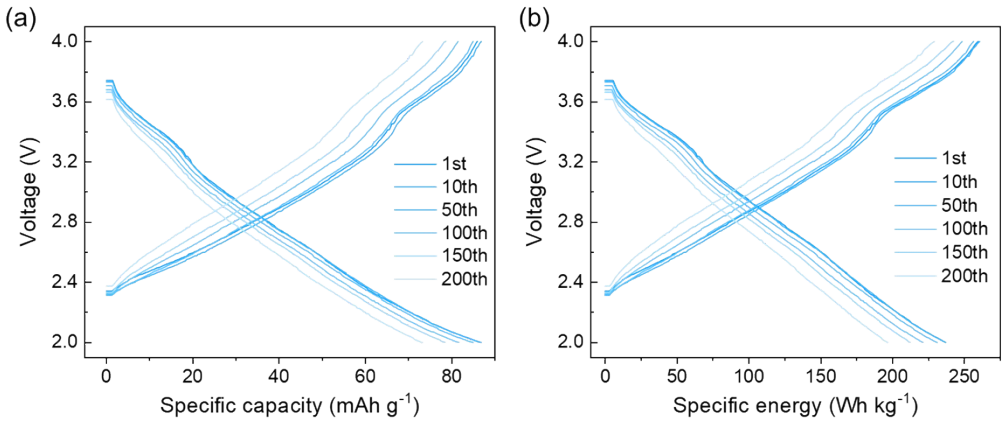

Figure S5. (a, b) Galvanostatic charge/discharge curves of NaMC-0.3 electrode versus specific capacity and energy in 1st, 10th, 50th, 100th, 150th, and 200th cycles at 5C, respectively.

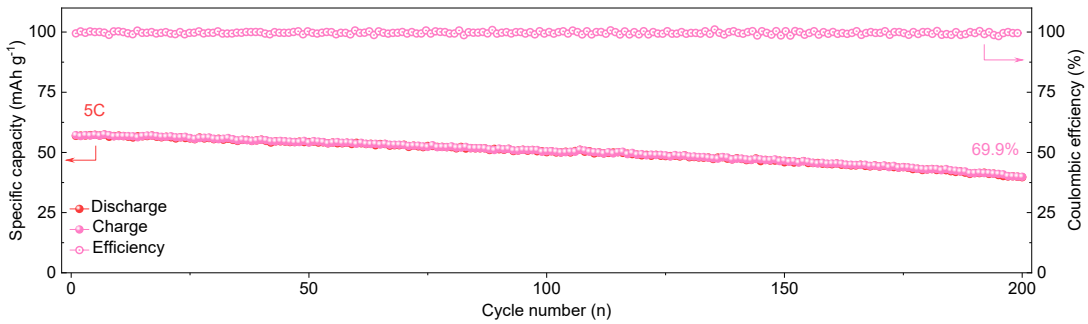

Figure S6. Cycling performance of NaMC-0.5 electrode during 200 cycles at 5C after various rates performance tests.

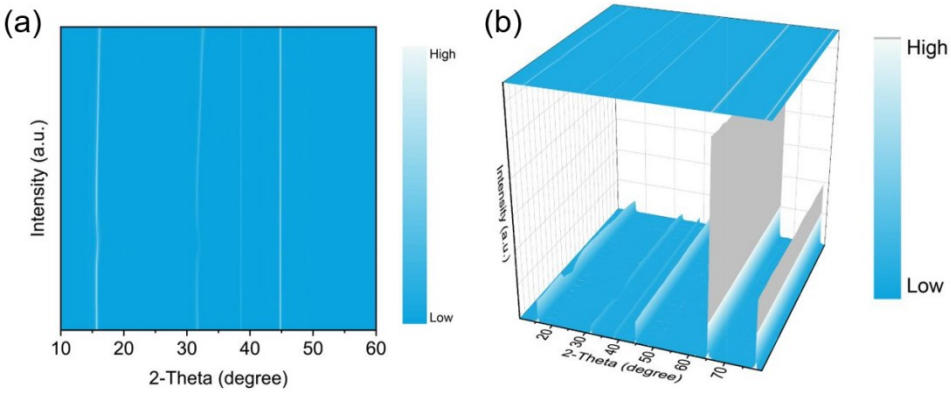

Figure S7. (a, b) The intensity contour maps (bird's eye view) and 3D counter graphs of NaMC-0.3 electrode during the first charge/discharge at 0.1 C in the voltage range of 2.0–4.0 V, respectively.

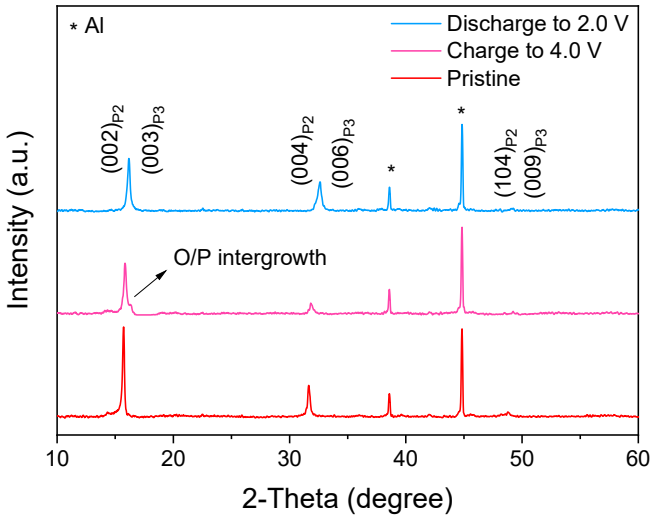

Figure S8. Detailed *in situ* XRD patterns of NaMC-0.3 electrode at different charge and discharge states.

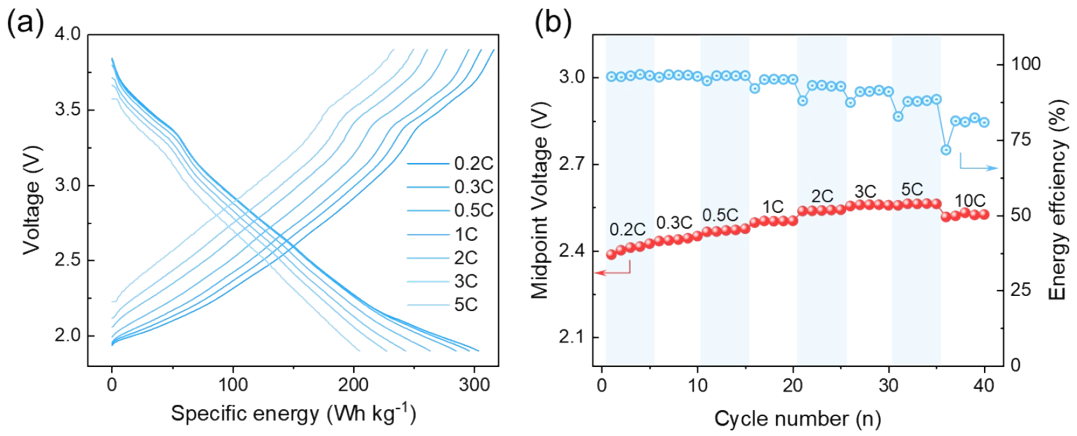

Figure S9. Rate performance for full-cell system. (a) Galvanostatic charge/discharge curves of NaMC-0.3 electrode versus specific energy at various rates in the voltage range of 1.9–3.9 V. (b) Corresponding Midpoint voltage as well as energy efficiency.

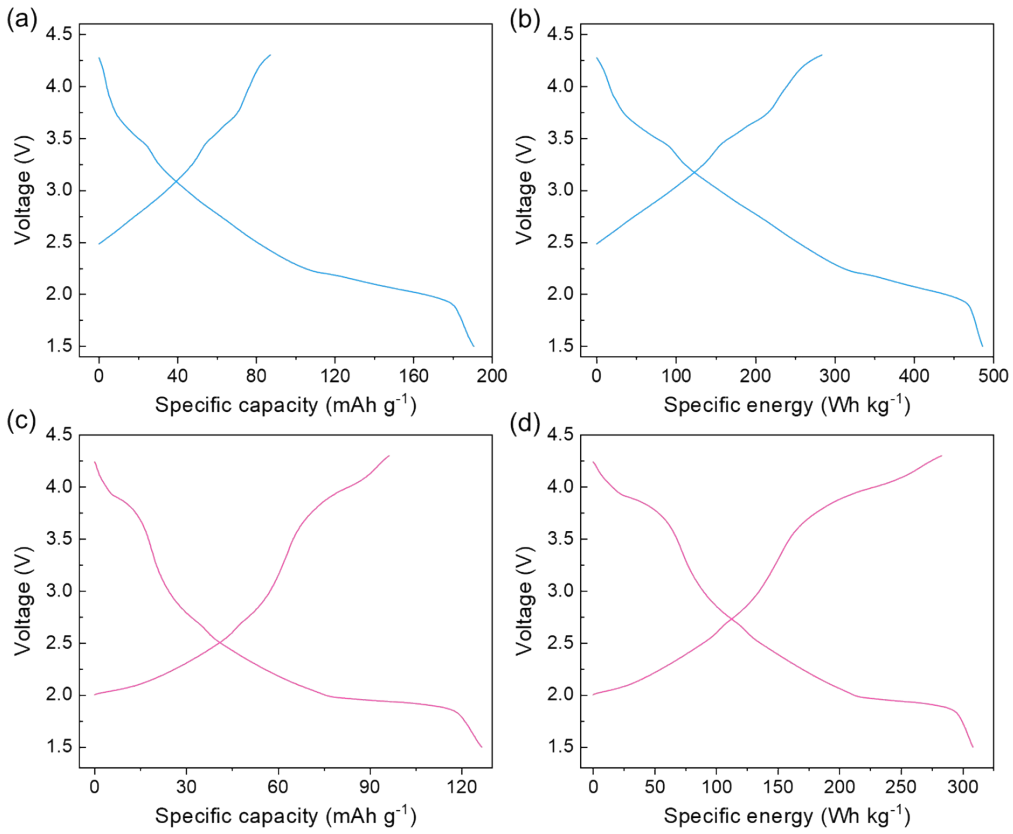

Figure S10. Initial galvanostatic charge/discharge curves for (a, b) NaMC-0.3 and (c, d) NaMC-0.5 electrodes in the voltage range of 1.5–4.3 V.

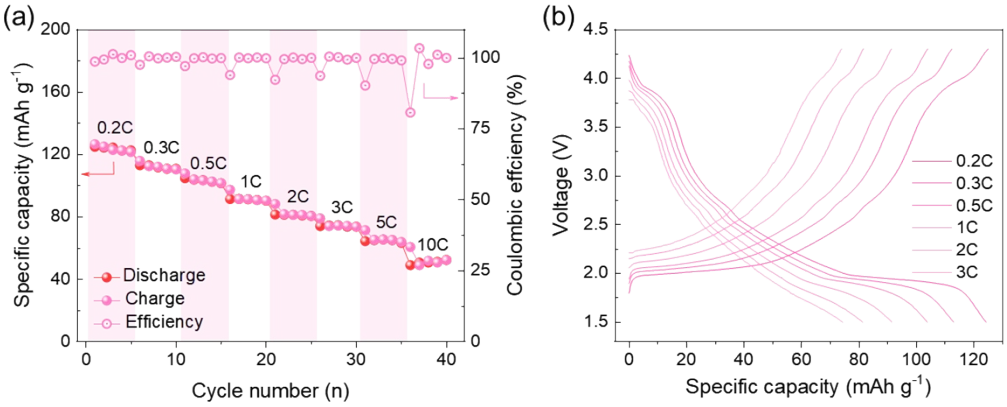

Figure S11. Electrochemical performance of NaMC-0.5 electrode in half-cell system within 1.5-4.3 V. (a, b) Rate performance and galvanostatic charge/discharge curves versus specific capacity at various rates, respectively.

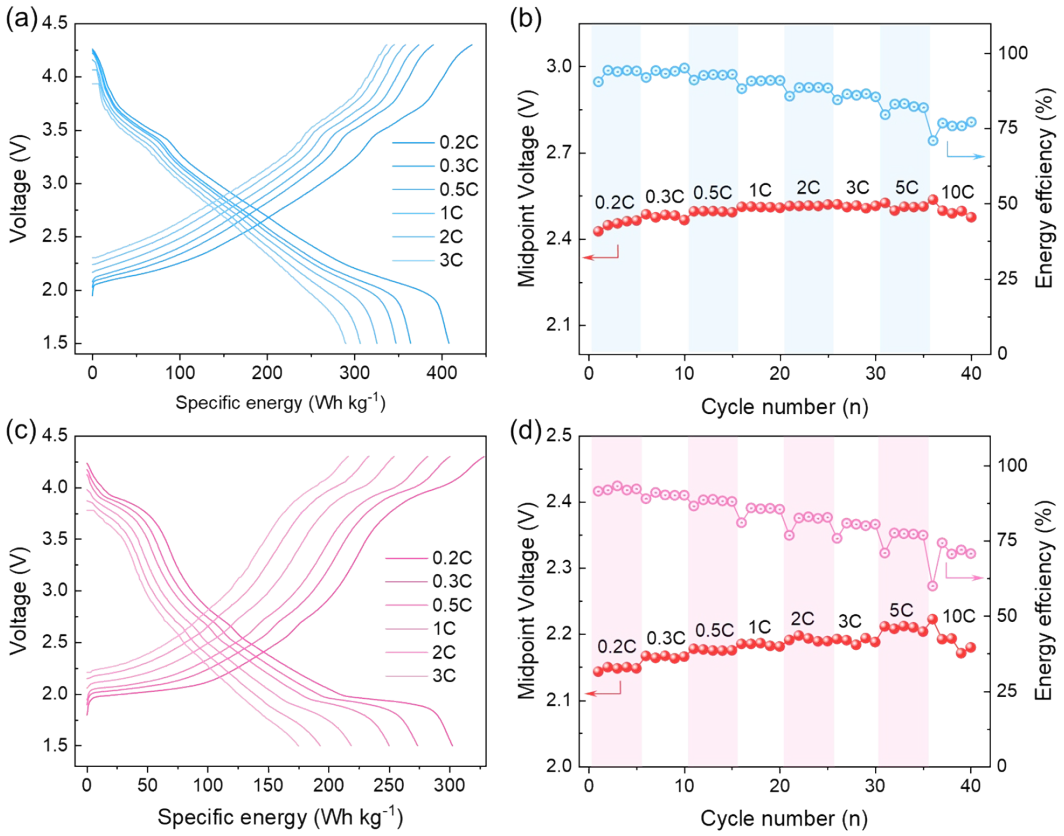

Figure S12. Rate performance for half-cell: Galvanostatic charge/discharge curves versus specific energy of (a) NaMC-0.3 and (c) NaMC-0.5 electrodes at various rates in the voltage range of 1.5-4.3 V, respectively. Corresponding midpoint voltage as well as energy efficiency of (b) NaMC-0.3 and (d) NaMC-0.5 electrodes.

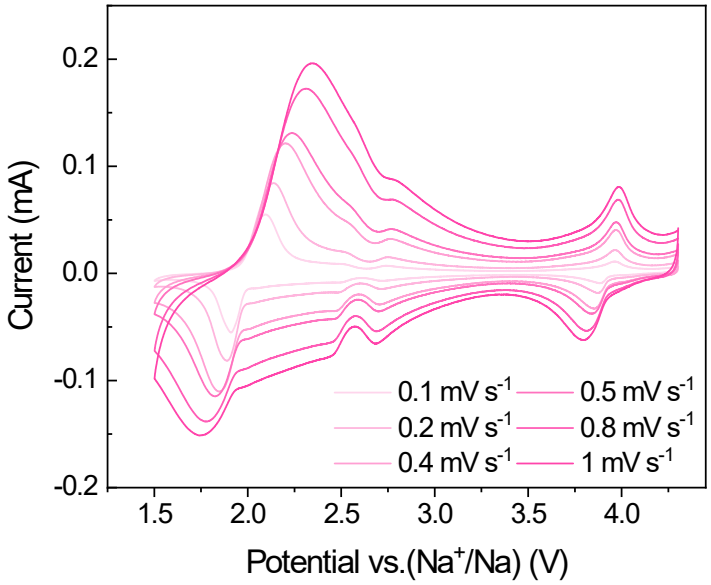

Figure S13. Cyclic voltammetry of NaMC-0.5 electrode at different scan rates.

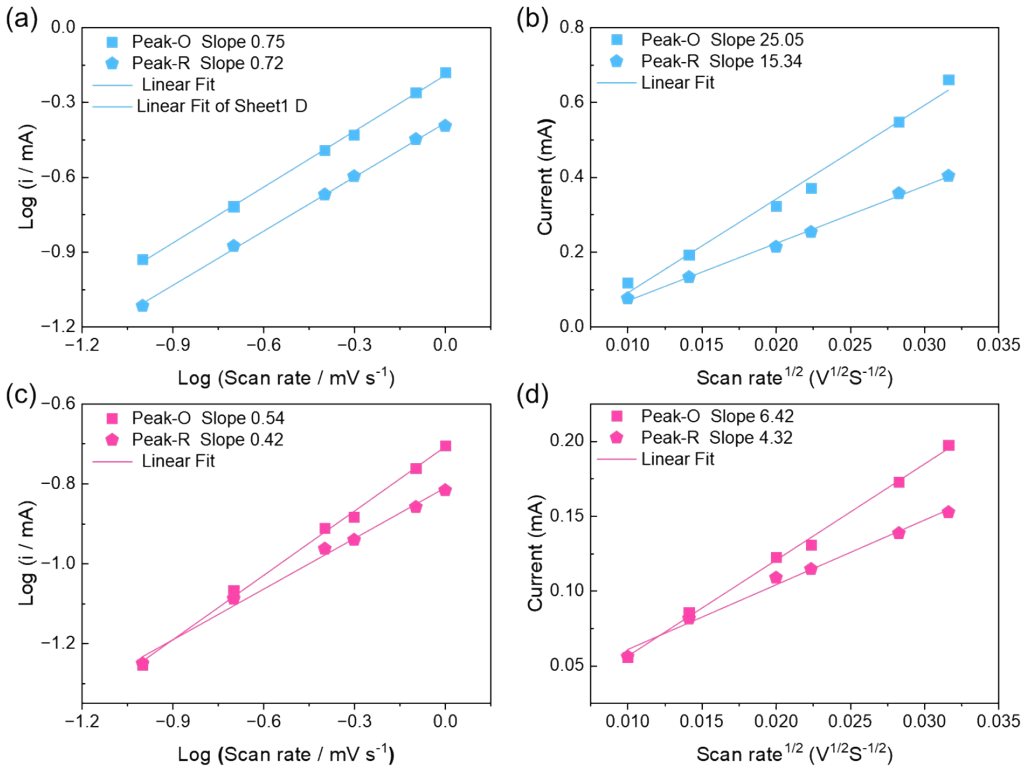

Figure S14. Linear fitting of log (*i*) versus log (*v*) plots and linear fitting of peak current versus square root of the scan rate of (a, b) NaMC-0.3, and (c, d). NaMC-0.5 electrodes, respectively.

Table S1. Summary of charge and discharge specific capacity (mAh g^{-1}) at different rates for NaMC-0.3 and NaMC-0.5 electrodes in half-cell system within 2.0-4.0 V.

Sample	0.2C	0.3C	0.5C	1C	2C	3C	5C	10C
NaMC-0.3	146.6/ 142.2	131.6/ 129.4	124.7/ 121.9	118.2/ 112.5	110.2/ 102.3	101.3/ 95.6	96.4/ 87.7	85.9/ 76.6
NaMC-0.5	71.2/ 69.6	70.3/ 69.3	66.0/ 65.5	61.5/ 60.9	61.2/ 60.3	59.6/ 58.7	57.6/ 56.5	56.5/ 53.9

Table S2. Summary of charge and discharge specific energy (Wh kg^{-1}) at different rates for NaMC-0.3 and NaMC-0.5 electrodes in half-cell system within 2.0-4.0 V.

Sample	0.2C	0.3C	0.5C	1C	2C	3C	5C	10C
NaMC-0.3	379.0/ 369.8	352.0/ 342.0	333.4/ 324.5	314.8/ 301.8	292.9/ 276.4	279.2/ 261.0	265.5/ 244.5	246.6/ 213.2
NaMC-0.5	198.3/ 188.3	195.2/ 188.2	183/ 177.4	170.8/ 165.0	169.3/ 162.9	166.0/ 158.9	160.7/ 153.2	154.6/ 146.0

Table S3. Comparison of structural features, chemical composition, synthesis methods, and electrochemical performance of reported similar cathode materials in half-cell systems.

Cathode materials	Synthesis methods	Current density	Discharge capacity	Rate performance	Cycle performance	Reference
P2/P3-$Na_{0.44}Mn_{0.7}Co_{0.3}O_2$	Thermal polymerization	1C=120 mA g^{-1}	142.2 mAh g^{-1} (0.2C, 2.0-4.0 V)	65.7% (5C/0.2C)	84.7% (200, 5C)	This work
P2/Tunnel-$Na_{0.44}Mn_{0.9}Co_{0.1}O_2$	Thermal polymerization	1C=120 mA g^{-1}	173.0 mAh g^{-1} (0.2C, 2.0-4.0 V)	62.0% (5C/0.2C)	82.0% (100, 5C)	Angew. Chem., Int. Ed., 2020, 59, 1491-1495.
P2-$Na_{0.44}Mn_{0.99}W_{0.01}O_2$	Solid-state reaction	1C=121 mA g^{-1}	180.0 mAh g^{-1} (0.2C, 2.0-4.0 V)	41.6% (5C/0.2C)	80.0% (200, 5C)	Adv. Energy Mater., 2023, 13, 2203802.
Tunnel-$Na_{0.44}Mn_{0.95}Mg_{0.05}O_2$	Solid-state reaction	1C=100 mA g^{-1}	105.0 mAh g^{-1} (0.2C, 2.0-3.8 V)	80.9% (5C/0.2C)	72.0% (800, 5C)	Adv. Sci., 2021, 8, 2004448.
Tunnel-$Na_{0.44}Mn_{0.98}Zr_{0.02}O_2$	oxalic acid solution	/	112.0 mAh g^{-1} (0.2C, 2.0-3.8 V)	89.2% (5C/0.2C)	80% (1000, 5C)	ChemElectroChem, 2020, 7, 2545-2552.
Tunnel-$Na_{0.44}Mn_{0.97}Al_{0.01}Ti_{0.01}Co_{0.01}O_2$	Solid-state reaction	/	136.0 mAh g^{-1} (0.2C, 2.0-4.0 V)	72.7% (5C/0.2C)	80% (2000, 10C)	Inorg. Chem. Front., 2023, 10, 841-849.
P2/Tunnel-$Na_{0.44}MnO_{1.93}F_{0.07}$	oxalic acid solution	/	165.0 mAh g^{-1} (0.2C, 2.0-4.2 V)	61.8% (5C/0.2C)	79% (400, 5C)	J. Power Sources, 2019, 427, 129-137.
P2/Tunnel-$Na_{0.44}Mn_{0.95}Ni_{0.05}O_2$	Solid-state reaction	1C=121 mA g^{-1}	112.0 mAh g^{-1} (0.2C, 2.0-4.0 V)	46.4% (2C/0.2C)	77.3% (100, 0.3C)	J. Solid State Chem., 2023, 318, 123741.
P2-$Na_{0.44}Mn_{0.89}Ni_{0.11}O_2$	Thermal polymerization	1C=120 mA g^{-1}	193.0 mAh g^{-1} (0.1C, 2.0-4.2 V)	47.0% (5C/0.1C)	74.0% (100, 0.1C)	J. Solid State Electro., 2019, 23, 2979-2988.
P2/Tunnel-$Na_{0.44}Mn_{0.89}Mg_{0.11}O_2$	Thermal polymerization		188.0 mAh g^{-1} (0.1C, 2.0-4.2 V)	51.0% (5C/0.1C)	81.0% (100, 0.1C)	

Table S4. Summary of charge and discharge specific capacity (mAh g^{-1}) at different rates for NaMC-0.3 and NaMC-0.5 electrodes in half-cell system within 1.5-4.3 V.

Sample	0.2C	0.3C	0.5C	1C	2C	3C	5C	10C
NaMC-0.3	168.7/ 159.6	146.7/ 142.6	138.0/ 134.6	130.0/ 125.5	122.1/ 118.1	116.7/ 113.5	111.0/ 105.2	104.5/ 95.0
NaMC-0.5	126.5/ 124.8	115.8/ 113.0	107.8/ 104.7	97.3/ 91.4	88.2/ 81.4	79.0/ 74.0	71.4/ 64.4	60.7/ 49.0

Table S5. Summary of charge and discharge specific energy (Wh kg^{-1}) at different rates for NaMC-0.3 and NaMC-0.5 electrodes in half-cell system within 1.5-4.3 V.

Sample	0.2C	0.3C	0.5C	1C	2C	3C	5C	10C
NaMC-0.3	434.2/ 407.9	390.0/ 364.1	373.5/ 347.3	358.2/ 325.6	345.5/ 306.5	336.7/ 290.0	324.8/ 270.6	301.8/ 229.0
NaMC-0.5	328.7/ 302.5	300.3/ 273.7	281.9/ 250.1	254.2/ 218.7	233.5/ 193.0	216.3/ 175.1	196.8/ 152.9	154.9/ 115.3